Experimental and Theoretical Study of State-Resolved Electronically Inelastic Collisions of Highly Rotationally Excited CN($A^2\Pi$) with Argon and Helium: The Role of Gateway Levels†

Boris Nizamov, Xin Yang,‡ and Paul J. Dagdigian*

Department of Chemistry, The Johns Hopkins University, Baltimore, Maryland 21218-2685

Millard H. Alexander

Department of Chemistry and Biochemistry, University of Maryland, College Park, Maryland 20742-2021

Received: December 31, 2001; In Final Form: March 20, 2002

A collaborative study of A → X electronic transitions from CN($A^2\Pi$,v=3,N=60−63) fine-structure Λ-doublet levels induced by collisions with argon and helium is presented. Experimental state-to-state rate constants were determined with an optical-optical double resonance technique. Specific levels of CN($A^2\Pi$,v=3,N=60−63) were prepared by excitation of the photolytically generated radical with a pulsed dye laser on various rotational lines in the $A^2\Pi-X^2\Sigma^+$ (3,0) band, and collisionally populated levels in the $v_A = 3$ and the nearly isoenergetic $v_X = 7$ vibronic manifolds were probed after a short delay by laser fluorescence excitation in the B−X (3,7) and B−A (3,3) bands. Final state distributions (relative state-to-state rate constants) are reported for CN(A)−Ar collisions; the rate constants for transitions induced by He were considerably smaller. Absolute total removal rate constants were also determined. A crossing of the $A^2\Pi$ $v = 3$ F_1f rotational/fine-structure manifold with the $X^2\Sigma^+$ $v = 7$ F_2 levels occurs at $J = 62.5$. The dependence of A → X rate constants and the total removal rate constants on the initial level demonstrates the importance of this "gateway" in facilitating collisions between these manifolds. The experimental CN(A)−Ar rate constants have been compared with theoretical rate constants computed in a quantum scattering treatment of the dynamics based on ab initio CN(A,X)−Ar potential energy surfaces. The small non-Born−Oppenheimer mixing of the A and X states in the isolated CN molecule was also included in the calculations. The computed total removal rates show an enhanced value for the perturbed $N = 62$ F_1f initial level, in agreement with experiment, but the computed state-to-state rate constants do not agree well with the experimentally determined values.

1. Introduction

An important collisional removal process for electronically excited molecules is electronic quenching to the ground electronic state. Rate constants have been measured for the electronic quenching of the excited electronic states of many diatomic and polyatomic molecules in collisions with a variety of targets. In part, interest in these rate constants has been stimulated by the application of laser diagnostic techniques, such as laser-induced fluorescence, for the measurement of concentrations of molecules and radicals in finite-pressure environments, such as flames and the atmosphere.[1,2] Because quenching affects the fluorescence quantum yield, and hence the relationship between signal strength and species concentration, knowledge of the quenching rate constants is crucial to a proper understanding of these experiments.

Two different mechanisms, which are not mutually exclusive, have been put forth to describe collision-induced electronic transitions.[3] The first mechanism is the "gateway" model of Gelbart and Freed,[4] which attributes transfer between different electronic states to spectroscopic perturbations in the diatomic moiety.[5] These perturbations mix the two states, with the result that collisions will allow interelectronic transitions to borrow from the large cross sections associated with rotationally inelastic scattering within a single electronic state.[6,7] Since spectroscopic perturbations are weak, the only levels that are accidentally nearly degenerate will mix significantly. Consequently, these sparse mixed levels should serve as gateways between the separate electronic states.

The second mechanism attributes collision-induced electronic transitions to the electrostatic mixing of the electronic states induced by the approach of the collision partner.[8] Implicit in the Gelbart−Freed model is the assumption that this coupling is weak. However, electrostatic coupling will enable collision-induced transitions between the two states even when spectroscopic perturbations between the two states are negligible, or forbidden by symmetry.

The application of modern laser techniques has allowed the state-to-state study of collision-induced rotational energy transfer in diatomic molecules, and collisions of a number of diatomic molecules in various electronic states have been studied with such techniques.[6,7] In contrast, there have been relatively few investigations of collision-induced electronic transitions in which both the initial and final rovibronic levels were resolved.[3] The paradigm for collision-induced electronic quenching has been the CN radical. The potential energy curve for the $A^2\Pi$ electronic state lies nested within the curve for the ground $X^2\Sigma^+$ state (see Figure 3 of ref 3), and there exist near degeneracies between rotational levels of the v_A vibronic manifold of the A

† Part of the special issue "Donald Setser Festschrift".

‡ Present address: Alliance for Nanomedical Technologies, 309 Stocking Hall, Cornell University, Ithaca, NY 14853.

10.1021/jp014691c CCC: $22.00
Published on Web 04/23/2002

state and the $v_X = v_A + 4$ manifold of the X state.[9] Individual levels in both electronic states can be probed conveniently by optical excitation to the $B^2\Sigma^+$ state.[10−12]

The non-Born−Oppenheimer perturbational mixing of the $A^2\Pi$ and $X^2\Sigma^+$ electronic states of CN has been well characterized by Kotlar et al.[9] Both mechanisms of energy transfer can thus be operative in CN A → X collisional transfer, unlike the situation for the isoelectronic N_2^+ ion,[13−16] for which there are no perturbations between the analogous $A^2\Pi_u$ and $X^2\Sigma_g^+$ states because of the g−u prohibition for perturbations in homonuclear diatomics.[5]

Collisional electronic energy transfer in the CN radical was first investigated by Pratt and Broida.[17] Other workers have investigated nonradiative electronic transfers in CN in Ne matrixes,[18] CN−Ne binary complexes,[19,20] CN−Ar_n clusters,[21] and in bimolecular collisions.[22,23] Dagdigian and co-workers[24−28] used optical-optical double resonance (OODR) to study electronic transitions from low rotational levels of the $v_A = 3$, 7, and 8 manifolds, induced by collisions with He and Ar. Unfortunately, in these studies any special role played by the perturbatively mixed gateway levels was obscured by the efficient electrostatic coupling between nonperturbatively mixed levels and by experimental difficulties in the direct laser excitation of the most perturbed A state levels[9,29] (in the $v_A = 7$ level).

On the basis of the theoretical work of Alexander and Corey,[8] Werner and co-workers[30] used multireference configuration (MRCI) techniques to generate the necessary potential energy surfaces (PESs) for the CNHe system. These were then used in quantum scattering studies to determine cross sections for various A → X transitions.[28,31] Overall, the agreement between the calculated and experimentally determined final state distributions was quite good.

More recently, again in collaboration with Werner, we reported similar MRCI PESs for the CNAr system.[32] We have used these to study pure rotational energy transfer within the A state.[32,33] In particular, using 193 nm photolysis of BrCN, rather than a discharge, to generate the CN radical, we were able to study collisions of CN($A^2\Pi$) in very high ($N \approx 60$) rotational levels of the $v_A = 3$ manifold with both Ar and He.[33,34] Although these experiments were limited to the study of rotational transitions within the A state, the same initial state preparation can be used to study electronic energy transfer emanating from these high rotational levels since the $v_A = 3$ and $v_X = 7$ manifolds cross in the range $J = 62.5-92.5$.[9] Because these levels are spaced far apart, electronic inelasticity arising from direct electrostatic coupling should be small, and spectral congestion should not be a problem. This would allow an unambiguous investigation of the role of perturbation-mixed gateways in electronic energy transfer, in particular through the perturbation at $J = 62.5$.

Figure 1 presents an energy level diagram for the $v_A = 3$ and $v_X = 7$ vibronic manifolds in the vicinity of this perturbation, which leads to mixed electronic state character (10% admixture) for the $v_A = 3$, $N = 62$ F_1f and $v_X = 7$, $N = 63$ F_2 levels. We report here the experimental measurement of total removal and A → X rate constants for collisions of $v_A = 3$, $N = 60$, 62, and 63 initial levels with Ar, and also with He. Initial levels that are both weakly and strongly affected by the isolated-molecule perturbation have been investigated in order to gauge the extent of the importance of the gateway levels. The experimental rate constants are compared with theoretical rate constants computed by quantum scattering methods based on the ab initio CN($X^2\Sigma^+$,$A^2\Pi$)−Ar PESs mentioned above.[32] The calculation of these rate constants explicitly includes the non-Born−Oppenheimer mixing of the $A^2\Pi$ and $X^2\Sigma^+$ states in the isolated CN radical.[9,28]

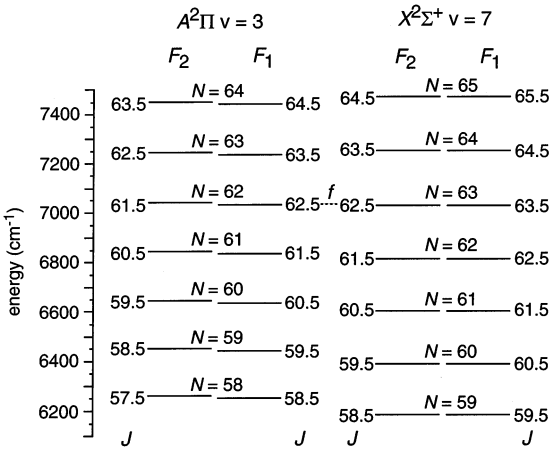

Figure 1. Energy level diagram of the CN $A^2\Pi$ $v = 3$ and $X^2\Sigma^+$ $v = 7$ vibronic manifolds around their crossing at $J = 62.5$. The levels are labeled with the total angular momentum J and the fine-structure labels F_1 and F_2, as well as the case (b) rotational angular momentum quantum number N. In the case (b) limit, $\mathbf{J} = \mathbf{N} + \mathbf{S}$ where $\mathbf{S}$ is the electron spin; we have $J = N + 1/2$ and $J = N - 1/2$ for F_1 and F_2 levels, respectively. Each rotational level in the $^2\Pi$ state is further split into the e and f Λ-doublets, of opposite total parity. The dotted line connecting the $N = 62$ F_1f level in the $A^2\Pi$ state and the $N = 63$ F_2 level in the $X^2\Sigma^+$ state denotes that these are the most perturbed levels in this energy range due to the non-Born−Oppenheimer mixing in the isolated diatom. From ref 9, we estimate that the $v_A = 3$, $N = 62$ F_1f level possesses 10% X state character, while the $v_X = 7$, $N = 63$ F_2 level possesses 10% A state character. The energies in the diagram are given relative to that of the CN($X^2\Sigma^+$,v=7,N=0) level.

2. Experimental Results

2.1. Apparatus. The experiments were carried out in the same apparatus as that used for the study of rotationally inelastic collisions of high CN($A^2\Pi$) rotational levels,[33,34] and the experimental arrangement is briefly described here. CN was produced in a quasi-static cell by 193 nm photolysis of BrCN (5 mTorr) diluted in He or Ar (total pressure 0.3−0.9 Torr). After a several microseconds delay to allow for translational equilibration,[35] a selected CN($A^2\Pi$) rovibrational/fine-structure level was excited by pulsed "pump" dye laser irradiation on isolated lines in the $A^2\Pi-X^2\Sigma^+$ (3,0) band. The populations of the initial level and collisionally populated levels in the $v_A = 3$ and $v_X = 7$ vibronic manifolds were probed by B → X fluorescence excitation in the $B^2\Sigma^+-A^2\Pi$ (3,3) and $B^2\Sigma^+-X^2\Sigma^+$ (3,7) bands 30 ns after the pump laser by a "probe" dye laser. The probe laser energy and A → X fluorescence induced by the pump laser were also recorded for normalization purposes while acquiring the OODR spectra.

As discussed previously,[33] the probe laser alone excited B → X fluorescence due to the presence of vibrationally excited CN($X^2\Sigma^+$) and electronically excited CN($A^2\Pi$) fragments from the photolysis and subsequent partial collisional relaxation. Hence, the pump laser was fired every other shot, and the laser on and off signals were separately summed over a preset number of shots before the probe laser was stepped to the next wavelength. OODR spectra for the determination of populations of collisionally populated levels were obtained by subtraction of these two signals. Typical OODR spectra with the pump laser on and off were presented previously (see Figure 2 of ref 33).

The initially prepared level in the $A^2\Pi$ state should have an isotropic M_J distribution since the A−X (3,0) band was saturated

TABLE 1: Total Removal Rate Constants (in 10^{-11} cm^3 molecule^{-1} s^{-1}) for Collisions of CN($A^2\Pi$,v=3) with Ar and He

initial level	% Σ character[a]	Ar (exp)	Ar (theory)[b]	Ar (theory)[c]	Ar (theory)[d]	He (exp)[e]
$N = 60$						
$F_1e(A')$[f]	1.3×10^{-2}	8.7 ± 0.4	8.08	6.21	7.15	19.0 ± 1.2
$F_2f(A')$	4.6×10^{-4}	9.1 ± 0.6			7.07	20.5 ± 0.9
$F_1f(A'')$	0.19	12.3 ± 1.7	10.82	9.50	10.5	20.7 ± 2.5
$F_2e(A'')$	2.1×10^{-3}	11.5 ± 1.1			10.8	20.9 ± 1.5
$N = 62$						
$F_1e(A')$	1.7×10^{-2}	9.5 ± 1.9	11.05	6.53		21.0 ± 1.1
$F_2f(A')$	4.7×10^{-4}	9.8 ± 2.0				20.7 ± 1.5
$F_1f(A'')$	10.4	17.5 ± 3.5	14.90	15.17		24.4 ± 1.6
$F_2e(A'')$	2.3×10^{-3}	10.7 ± 2.1				19.0 ± 1.1
$N = 63$						
$F_1e(A')$	2.0×10^{-2}	12.2 ± 1.5				
$F_2f(A')$	4.7×10^{-4}	9.6 ± 0.9				
$F_1f(A'')$	1.6	14.1 ± 1.2				
$F_2e(A'')$	2.4×10^{-3}	9.8 ± 0.8				

[a] Computed from the Hamiltonian of Kotlar et al.[9] [b] Computed with the four diabatic CN($A^2\Pi$, $X^2\Sigma^+$)−Ar PESs[32] and the isolated-molecule spectroscopic perturbation.[9] [c] Computed with the coupling PES V_1 set to zero, but with the isolated-molecule perturbation. [d] Computed with the CN($A^2\Pi$)−Ar PESs V_Π and V_2,[32] and hence only includes rotationally inelastic transitions within the A state. [e] Reference 34. [f] The reflection symmetry[37] of the initial levels is given in parentheses.

at the 5 mJ pulse energy at which the pump laser was usually operated. Care was taken to adjust the energy of the probe laser beam so that excitation of the both the B−A (3,3) and B−X (3,7) bands were in the linear regime. It should be noted that the band strength of the former is considerably larger than that of the latter[36] so that saturation effects would tend to lead to an overestimate of the rotational populations in the X state vs those in the A state. The OODR spectra were recorded at probe laser pulse energies of approximately 30 μJ. A discussion of the intensity factors for converting the B ← A and B ← X laser-induced fluorescence signals to populations is presented in the Appendix.

2.2. Total Removal Rate Constants. A first test of the importance of the gateway mechanism is to see whether the rate constants for depletion of the population of the initially excited $A^2\Pi$ level by all collisional processes is enhanced at a spectroscopic "gateway."

The total removal rate constants were determined in the following manner, as described in detail previously.[32,33] The intensities of parent lines in the OODR spectra, which are a measure of the concentrations of the initially prepared $A^2\Pi$ levels, were recorded as a function of the pump−probe delay and were fitted to a single-exponential decay. Rate constants were computed from averages of the results from three to four runs. The total removal rate constants can be equated with the sum of the rate constants for collision-induced rotational and electronic transitions since other processes such as diffusion occur on a much longer time scale.

We have investigated collisions of CN($A^2\Pi$,v=3,N=60,62,-63) fine-structure/Λ-doublet levels. These initial levels lie both below and above the most perturbed level, with $J = 62.5$. The experimentally determined total removal rate constants are presented in Table 1. The reflection symmetries[37] and the fractional Σ-state character of the initial fine-structure/Λ-doublet levels are also indicated. The rate constants for CN(N=60)−Ar and CN−He collisions were reported previously.[33,34] The overall differences in the magnitudes of the rate constants for CN−He vs CN−Ar collisions have been discussed previously.[34] The total removal rate constants for collisions with He show no dependence upon the fine-structure label or Λ-doublet symmetry of the initial level, with the exception of the perturbed $N = 62$ F_1f level, for which the total removal rate constant is approximately 20% higher than for the other levels.

As noted previously,[33] the total removal rate constants for the essentially unperturbed $N = 60$ levels in collisions with Ar are approximately 35% higher for Λ-doublet levels of A″ symmetry than for A′ initial levels. These differences were shown[33] to be due to differences in the total rotational energy transfer rates out of the Λ-doublet levels of different reflection symmetries because of the Λ-doublet specificities in the rotationally inelastic collision dynamics. For the $N = 62$ levels, the total removal rate constant for the perturbed F_1f level is seen to be approximately 75% larger than the corresponding rate constants for the other $N = 62$ initial levels. This, and the previously noted enhanced total removal rate constant for this level in collisions with He, strongly suggests that the energy transfer rate out of the perturbed level is being enhanced because of the spectroscopic perturbation, presumably through enhanced A → X collisional transfer. The total removal rate constant for the slightly perturbed $N = 63$ F_1f level is seen to be 15−45% larger than for the other $N = 63$ levels in CN−Ar collisions.

2.3. OODR Spectra. State-to-state rate constants for collision-induced electronic transitions of $N = 60$, 62, and 63 levels with Ar as the collision partner were determined from line intensities in OODR spectra. In previous work,[33,34] we reported experimental and computed state-to-state rate constants for collision-induced rotational transitions within the $A^2\Pi$ state for the $N = 60$ levels for both Ar and He as collision partners. In the present work, we have also investigated A → X transitions induced through collisions with He. The A → X rate constants for the latter system are found to be much smaller, as evidenced by the smaller enhancement of the total removal rate constant for the perturbed $N = 62$ F_1f level, noted in the previous section, and as expected from the smaller A ∼ X coupling PES for the CN−He system compared with CN−Ar.[30,32] Hence, a much less extensive study of CN−He collision-induced transitions was carried out. Below we first describe our observations for CN−Ar collisions.

Figure 2 presents portions of the OODR spectra for which the $N = 60$ F_1e and F_1f levels were initially prepared by pump laser irradiation on the A−X (3,0) $R_1(59)$ and $Q_1(60)$ lines, respectively. In addition to the B−A $Q_1(61)$ and $Q_2(61)$ lines involving detection of CN molecules that have undergone $\Delta N = +1$ rotationally inelastic transitions, we observe in each spectrum one B−X line, indicative of a collision-induced A → X electronic transition. Similar OODR spectra were observed for the $N = 60$ Λ-doublet levels in the F_2 fine-structure manifold. For initial Λ-doublet levels of A′ reflection symmetry (F_1e and F_2f), a $\Delta N = +1$ transition populated the observed rotational level in the $X^2\Sigma^+$ state; this transition is accompanied by very

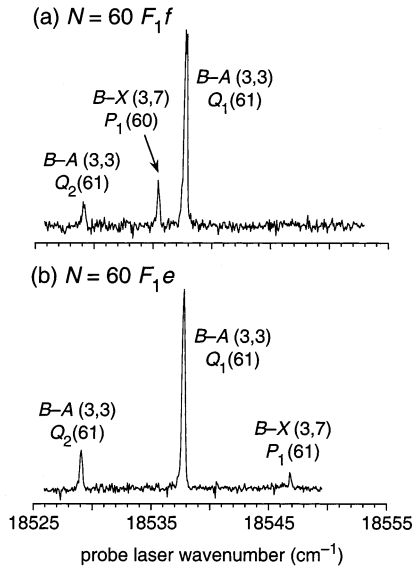

Figure 2. Probe laser fluorescence excitation spectra with the pump laser tuned to the (a) $Q_1(60)$ and (b) $R_1(59)$ lines of the $A^2\Pi-X^2\Sigma^+$ (3,0) band ($N = 60$ F_1f and F_1e levels, respectively, initially prepared) in the presence of 500 mTorr Ar and 5 mTorr BrCN. The pump−probe delay was 30 ns. Lines in the $B^2\Sigma^+-A^2\Pi$ (3,3) and $B^2\Sigma^+-X^2\Sigma^+$ (3,7) bands are identified.

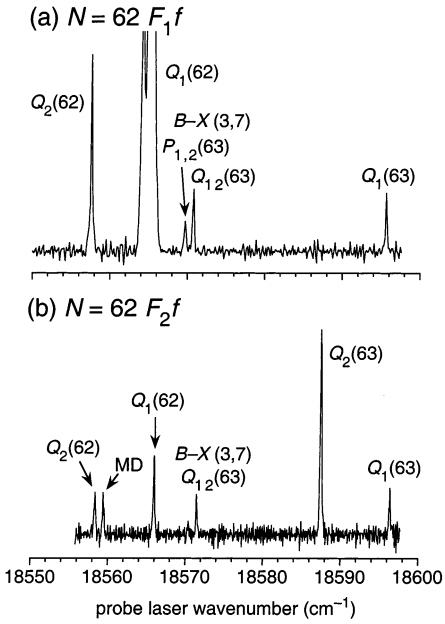

Figure 3. Probe laser fluorescence excitation spectra with the pump laser tuned to the (a) $Q_1(62)$ and (b) $R_2(61)$ lines of the $A^2\Pi-X^2\Sigma^+$ (3,0) band $N = 62$ F_1f and F_2f levels, respectively, initially prepared) in the presence of 500 mTorr Ar and 5 mTorr BrCN. The pump−probe delay was 30 ns. Lines in the $B^2\Sigma^+-A^2\Pi$ (3,3) and $B^2\Sigma^+-X^2\Sigma^+$ (3,7) bands are identified. The line denoted "MD" is a magnetic dipole transitions in the B−A band (see ref 38).

little change in the CN internal energy (see Figure 1). In contrast, a $\Delta N = 0$ transition populated the observed X state level for initial Λ-doublet levels of A″ reflection symmetry (F_1f and F_2e), with the loss of approximately 200 cm^{-1} of internal energy. In all cases, the fine-structure label was conserved in the collision-induced electronic transition.

The OODR spectra for the $N = 62$ manifold indicate a significantly different collisional behavior for these fine-structure/Λ-doublet initial levels than for the $N = 60$ levels. Figure 3 presents OODR spectra for the perturbed F_1f initial level, as well as the F_2f level, in the spectral region where B−X lines were observed. Lines in the B−A (3,3) and B−X (3,7) bands are observed. As discussed in detail previously,[38] one of the lines in the spectra is a B−A magnetic dipole transition out of the initially prepared A state level.

For one of the $N = 62$ initial Λ-doublet levels, i.e., the perturbed F_1f level, the intensities of lines in the P branch of the B−X (3,7) band at $N = 63$ are large. As seen in Figure 1, the most perturbed level in the $v_X = 7$ manifold is the $N = 63$ F_2 level. The A ∼ X mixing has a dramatic effect on lines associated with $N = 63$ in the P branch of the B−X (3,7) band. As Figure 4 shows, there are three electric-dipole allowed lines in the P branch of a $^2\Sigma^+-^2\Sigma^+$ transition, e.g., a CN B−X band, for each rotational manifold N in the lower $^2\Sigma^+$ state.[39] Normally, the "satellite" Q_{12} line has negligible intensity for high N.[39] Thus, in CN B−X bands at high N, each member of the P branch usually consists of two lines, P_1 and P_2 (see Figure 2), which are resolved because the spin splitting in the B state is larger than that in the X state.[10,12] However, for $v_X = 7$ $N = 63$, the A ∼ X mixing leads to an intensity factor for the B−X (3,7) $Q_{12}(63)$ line that is approximately twice that of the $P_1(63)$ line. Moreover, the perturbation leads to a larger energy separation of the $N = 63$ F_1 and F_2 levels, which is approximately equal to the spin splitting in the B state. This implies that the $P_1(63)$ and $P_2(63)$ lines are overlapped and the $Q_{12}(63)$ line appears at slightly higher wavenumber. These considerations were taken into account in deriving state-to-state rate constants, which are presented in the next subsection.

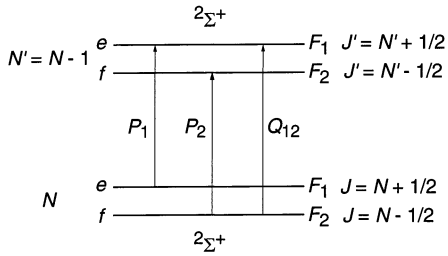

Figure 4. Allowed rotational lines in the P branch of a $^2\Sigma^+-^2\Sigma^+$ electronic transition.

Figure 5 presents OODR spectra for which the $N = 63$ F_1f and F_2f levels were initially prepared by pump laser irradiation on the A−X (3,0) $R_1(62)$ and $R_2(62)$ lines, respectively. In addition to lines in the B−A Q_1 and Q_2 branches, involving detection of the initial level and levels populated by collision-induced rotational transitions, we see B−X lines associated with the $N = 64$ rotational manifold N in the X state, indicative of collision-induced electronic transitions to the $v_X = 7$ vibronic manifold.

As discussed previously,[34] the signal-to-noise ratio in OODR spectra probing CN−He collisions was poorer than for CN−Ar collisions since rotational relaxation of high rotational levels of $CN(X^2\Sigma^+)$ is faster with He than with Ar.[40] As a result of the poorer signal-to-noise ratio and the smaller A → X collision-induced electronic transfer rates for CN−He collisions, suggested by the state dependence of the total removal rate constants presented in section 2.2, an extensive study of the CN−He state-to-state electronic energy transfer rates was not carried out. In fact, A → X collisional transfer was definitely observed only for the perturbed $N = 62$ F_1f level. Figure 6 presents an OODR spectrum for pump laser excitation of this level by irradiation on the A−X (3,0) $Q_1(62)$ line. Collisional population of the $v_X = 7$, $N = 63$ fine-structure levels can be inferred from observation of the B−X (3,7) $P_{1,2}(63)$ and $Q_{12}(63)$ lines, in

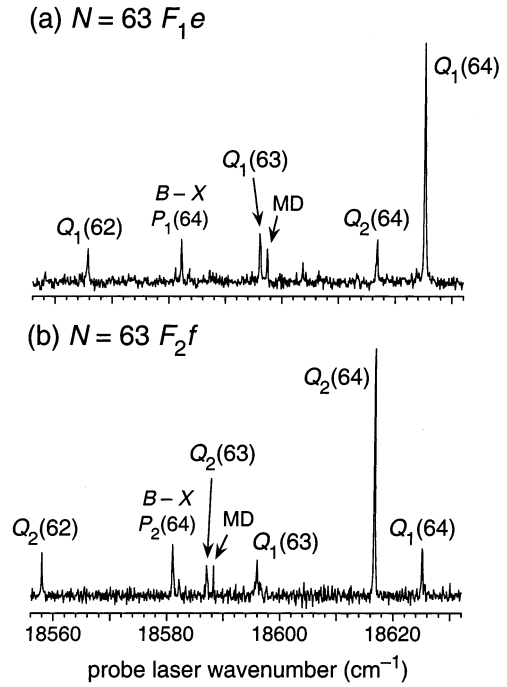

Figure 5. Probe laser fluorescence excitation spectra with the pump laser tuned to the (a) $R_1(62)$ and (b) $R_2(62)$ lines of the $A^2\Pi-X^2\Sigma^+$ (3,0) band ($N = 63$ F_1e and F_2f levels, respectively, initially prepared) in the presence of 500 mTorr Ar and 5 mTorr BrCN. The pump−probe delay was 30 ns. Lines in the Q_1 and Q_2 branches of the $B^2\Sigma^+-A^2\Pi$ (3,3) band, as well as the $P_{1,2}(64)$ lines of the $B^2\Sigma^+-X^2\Sigma^+$ (3,7) band, are identified. Magnetic dipole transitions from the initially prepared levels are denoted "MD" (see ref 38).

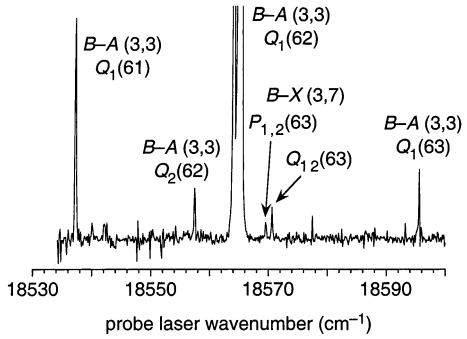

Figure 6. Probe laser fluorescence excitation spectrum with the pump laser tuned to the $Q_1(62)$ line of the $A^2\Pi-X^2\Sigma^+$ (3,0) band ($N = 62$ F_1f initial level prepared) in the presence of 300 mTorr He and 5 mTorr BrCN. The pump−probe delay was 30 ns. Lines in the $B^2\Sigma^+-A^2\Pi$ (3,3) and $B^2\Sigma^+-X^2\Sigma^+$ (3,7) bands are identified.

analogy to the observations for collisions of this initial level with Ar.

Comparison of the intensities of the B−X $P_{1,2}(63)$ and Q_{12}-(63) lines in the OODR spectra displayed in Figures 3a and 6 for collisions of the $N = 62$ F_1f level with Ar and He, respectively, to gauge the relative magnitudes of the A → X rate constants can be misleading. For both collision partners, the intensities of the B−X lines relative to the B−A $Q_1(62)$ line are similar. The latter line probes a level formed by fine-structure changing rotationally inelastic collisions. This process has a much smaller rate constant for CN(A)−He than for CN-(A)−Ar collisions.[20,34]

2.4. Relative State-to-State Rate Constants. From OODR spectra such as those shown in Figures 2, 3, 5, and 6, final rotational state distributions (relative state-to-state rate constants) for collision-induced electronic transitions to the $v_X = 7$ manifold were determined. In all cases, the pump−probe delay was 30 ns. From the total removal rate constants given in the previous section, the population of the initially prepared level in the A state was reduced from its initial value by less than 10% for this delay. Under these conditions, transfer between the initial level and a final level through secondary collisions involving intermediate levels is negligible since the populations of the collisionally populated levels are considerably less than that of the initially prepared level.

Intensity factors, required for the conversion of relative intensities in the OODR spectra to relative state-to-state rate constants, for lines in both the B−A (3,3) and B−X (3,7) bands were computed using spectroscopic constants of Kotlar et al.[9] for the mixed $v_A = 3$ and $v_X = 7$ manifolds. The non-Born−Oppenheimer mixing of these manifolds[9] was explicitly included in the calculation of the intensity factors.[41] The Appendix presents our estimation of the ratio of the electric dipole transition matrix elements $\mu(v_B=3,v_X=7)/\mu(v_B=3,v_A=3)$, required to put the intensity factors in the B−A and B−X bands on the same scale. Some comment about the determination of the populations in the $v_X = 7$, $N = 63$ F_1 and F_2 fine-structure levels is in order, given the spectral overlap of the B−X (3,7) $P_{1,2}(63)$ lines noted above. The population in the F_2 level was determined from the intensity of the $Q_{12}(63)$ line, which is free from overlap. The population in the F_1 level was then determined from the intensity attributable to the $P_1(63)$ line in the overlapped $P_{1,2}(63)$ pair, after subtraction of the computed intensity for the $P_2(63)$ line.

The final state distributions for collision-induced electronic transitions into the $v_X = 7$ manifold were normalized so that the population of the final level corresponding to the $\Delta N = -1$ fine-structure and Λ-doublet symmetry conserving collision-induced pure rotational transition within the $v_A = 3$ manifold equals unity. Thus, the magnitudes of collision-induced electronic and rotational transitions can be directly compared.

Table 2 presents the experimentally determined relative state-to-state for collision-induced A → X electronic transitions from the $N = 60$, 62, and 63 fine-structure/Λ-doublet levels in the $v_A = 3$ manifold for Ar as the collision partner. For each initial level, two to three spectra were recorded to obtain relative state-to-state rate constants and statistical errors. The relative rate constants are normalized by setting the value for the $\Delta N = -1$ fine-structure and Λ-doublet symmetry conserving pure rotational transition within the $v_A = 3$ manifold to unity. For convenience, we have indicated in Table 2 the reflection symmetries[37] of the initial levels. In previous work,[33] we reported the relative state-to-state rate constants for collision-induced rotational transitions within the A state for $N = 60$ initial levels.

In the case of collisions of the relatively unperturbed $N = 60$ initial levels, only one collisionally populated level within the X state could be detected, and the relative rate constants for the other final levels were below our detection limit (see Figures 2, 3, 5, and 6). As noted previously,[33] the CN(A) levels at this high level of rotational excitation lie close to the Hund's case (b) limit, and this is reflected in the propensities for collisionally populating specific rotational levels within the X state. We see from Table 2 that the fine-structure label is conserved in these A → X collision-induced electronic transitions. This implies that the coupling of the rotational angular momentum **N** and electron spin **S** to form the total angular momentum **J** is maintained.

We also see that initial Λ-doublet levels of A′ symmetry preferentially yield the rotational level in the X state with ΔN

TABLE 2: Experimentally Determined Relative State-to-State Rate Constants[a] for A → X Electronic Transitions from CN($A^2\Pi$,v=3,N) Fine-Structure/Λ-Doublet Levels Induced by Collisions with Ar

	initial fine-structure/Λ-doublet level			
final level	F_1e (A′)[b]	F_2f (A′)	F_1f (A″)	F_2e (A″)
	$N = 60$ Initial Levels			
$N' = 60$				
F_1			0.93 ± 0.19	
F_2				0.40 ± 0.07
$N' = 61$				
F_1	0.34 ± 0.06			
F_2		0.27 ± 0.05		
sum[c]	0.34	0.27	0.93	0.40
	$N = 62$ Initial Levels			
$N' = 62$				
F_1				b
F_2				b
$N' = 63$				
F_1	0.93 ± 0.20	0.11 ± 0.02	0.46 ± 0.09	0.24 ± 0.04
F_2	0.19 ± 0.04	0.79 ± 0.16	2.56 ± 0.45	0.84 ± 0.17
sum[c]	1.12	0.90	3.02	1.08
	$N = 63$ Initial Levels			
$N' = 63$				
F_1			1.40 ± 0.19	
F_2			0.31 ± 0.05	0.73 ± 0.14
$N' = 64$				
F_1	0.97 ± 0.11	0.37 ± 0.14	0.58 ± 0.10	0.50 ± 0.10
F_2	0.32 ± 0.09	0.85 ± 0.13	0.96 ± 0.13	0.27 ± 0.05
sum[c]	1.29	1.22	3.25	1.50

[a] Normalized to the $\Delta N = -1$ fine-structure and Λ-doublet symmetry conserving collision-induced pure rotational transition within the $v_A = 3$ manifold. Blank entries in the table indicate that the final level was not detected in the OODR spectra. [b] Final level could not be detected because of a spectral overlap. [c] Sum of the relative rate constants over the final levels.

$= +1$, and little change in the CN internal energy (see Figure 1), while initial levels A″ symmetry form the X state level with $\Delta N = 0$, and consequently loss of ca. 200 cm^{-1} of internal energy. Analogous Λ-doublet propensities were observed in rotationally inelastic CN(A)−Ar collisions.[33] In this case, the Λ-doublet levels of A′ symmetry underwent $\Delta N = +1$ collision-induced rotational transitions to final levels of A″ symmetry, while Λ-doublet levels of A″ symmetry underwent $\Delta N = -1$ collision-induced rotational transitions to final levels of A′ symmetry. From the relative A → X state-to-state rate constants given in Table 2 and those given previously[33] for pure rotational transitions within the A state, we find that the rate constants for A → X transitions are approximately 10−15% of the sum of the rate constants for all pure rotational transitions.

The A → X state-to-state rate constants for $N = 62$ and 63 initial levels show some qualitative differences with the $N = 60$ rate constants. Table 2 does show that the Λ-doublet levels of A′ symmetry, which are relatively unaffected by the A ∼ X perturbation (see Table 1), show a marked propensity for formation of X state levels with a $\Delta N = +1$ change in the rotational angular momentum and conservation of the fine-structure label, exactly as found for the corresponding $N = 60$ initial levels. However, the relative rate constants for the $N = 62$ and 63 levels are larger than for the $N = 60$ initial levels.

The final state distributions in the case of the $N = 62$ and 63 Λ-doublet initial levels of A″ symmetry differ considerably from those found for the $N = 60$ A′ levels. There does not appear to be strong propensity to populate X state levels with $\Delta N = 0$ and conservation of the fine-structure label, as in the case of the corresponding $N = 60$ levels. For the $N = 62$ A″ initial levels, there are large rate constants for formation of the $N = 63$ levels in the X state, with a preference for formation of the F_2 over the perturbed F_1 fine-structure level. In the case of the $N = 63$ A″ initial levels, there is roughly equal population of the $N = 63$ and 64 rotational levels in the X state. We also see that the sum of the A → X rate constants into all final rotational levels are larger than for the $N = 60$ initial levels, particularly for the F_1f levels, which are those most strongly affected by the A ∼ X perturbation.[9] These enhanced A → X rate constants are consistent with the larger total removal rate constants reported in section 2.2 for the $N = 62$ and 63 F_1f initial levels.

From OODR spectra such as that shown in Figure 6, we have also determined the relative state-to-state rate constants for collision-induced electronic transitions out of the perturbed $N = 62$ F_1f level for He as the collision partner. As noted in section 2.3, this was the only initial level for which collisionally populated levels in the X state could be detected for CN(A)−He collisions. The only observed final levels are the $v_X = 7$, $N = 63$ F_1 and F_2 fine-structure levels, produced with relative rate constants of 0.08 ± 0.02 and 0.18 ± 0.04, respectively. As in the case of CN−Ar collisions, these CN−He rate relative rate constants were normalized to the $\Delta N = -1$ fine-structure and Λ-doublet symmetry conserving pure rotational transitions. We also see a preferential population of the perturbed F_2 final "gateway" level, as in the case of collisions with Ar. However, it can be seen by comparison with the CN−Ar state-to-state rate constants reported in Table 2 that the magnitude of the A → X rate constants, relative to the pure rotational energy rate constants, are approximately an order of magnitude smaller for CN(A)−He than for CN(A)−Ar collisions.

3. Theoretical Calculations

3.1. Formalism. The calculation of state-to-state cross sections and thermal rate constants for collision-induced $^2\Pi \rightarrow {}^2\Sigma^+$ electronic transitions follows the formalism we have presented previously.[28,32,42] The total wave function of the CN-($A^2\Pi$,$X^2\Sigma^+$)−Ar system is expanded as a sum of products of the molecular electronic-rotational wave functions, expressed in an intermediate coupling scheme, multiplied by functions that describe the orbital motion of the argon atomic collision partner with respect to the diatomic molecule. For the $^2\Pi$ rotational levels under consideration here ($N \approx 60$), the molecular wave functions are close to the Hund's case (b) limit, in contrast to low rotational levels, which follow case (a) coupling. The asymptotic dependence of the expansion coefficients describing the contribution of each diatomic internal and orbital basis function defines the fundamental scattering S matrix.

As in our previous studies of collision-induced rotational transitions of CN($A^2\Pi$) $N \approx 60$ rotational levels with Ar and He,[33,34] the computationally faster coupled-state (CS) approximation,[43] rather than the full close-coupling method, was used. The CS approximation utilizes a body-frame (BF) expansion of the wave function,[44,45] in which **P** denotes the BF projection of **J**.[46] In the BF expansion the matrix of the orbital angular momentum **L** is not diagonal. In the CS approximation, the off-diagonal matrix elements of **L** are set to zero, and the diagonal centrifugal terms[45] are replaced by the diagonal matrix $\hbar^2\bar{L}(\bar{L}+1)/2\mu R^2$, where $\bar{L}$ is an effective orbital angular momentum, taken to be the same for all channels.

Since **L** must be perpendicular to the triatomic plane, **P** is hence also the projection of the total angular momentum **J** along **R**, the vector connecting the atom and center of mass of the diatom. In the CS approximation, it is assumed that the projection **P** does not change during the collision. This, in turn, implies that the angle between the plane of rotation, which

becomes increasingly better defined for high J, and the vector **R** is also conserved.

The application of the CS method to collision-induced $^2\Pi \rightarrow {}^2\Sigma^+$ electronic transitions involving a diatomic molecule and an atomic collision partner has been described earlier.[28] In particular, we have presented explicit expression for the matrix elements of the interaction potential involving a Π electronic state in intermediate case coupling, with inclusion of the non-Born−Oppenheimer mixing of the isolated-molecule diatomic electronic/rotational states. After the scattering calculation, thermal rate coefficients were obtained by integrating the computed state-to-state cross sections over an assumed Boltzmann distribution of relative collision energies.[47]

3.2. Computed Rate Constants. The relative importance of the two mechanisms for collision-induced electronic transitions, involving the spectroscopic "gateway" and/or direct electrostatic coupling induced by the approach of the perturber, was computationally investigated through calculations of state-to-state rate constants from a selected set of initial $v_A = 3$ levels, including the most strongly perturbed $N = 62$ F_1f level. Specifically, we computed state-to-state and total removal rate constants involving F_1e and F_1f initial levels for $N = 60$ and 62, for which rate constants were also experimentally determined. The size of the state expansion, as well as the integration parameters and maximum value of the total angular momentum **J**, were chosen to ensure an accuracy of better than 1% in the calculated probabilities for all transitions out of these initial levels. All scattering calculations were performed with our HIBRIDON code.[48]

The matrix elements of the interaction potential were calculated using the computed CN($X^2\Sigma^+$, $A^2\Pi$)Ar PESs of Berning and Werner.[32] It should be pointed out that in a diabatic basis four PESs are needed.[42] Two of these, V_Π and V_2, describe the interaction of the Π state with the atomic target, while a third, V_Σ, describes the interaction of the Σ^+ state with the atom. Finally, V_1 represents the electrostatic coupling of the A′ component of the Π state with the Σ^+ state, which is induced by the approach of the atom. In the calculation of state-to-state rate constants, integral inelastic cross sections were carried out at 36 collision energies that spanned the range 5 $cm^{-1} < E <$ 2005 cm^1. The most probable collision energy in thermal experiments at $T = 295$ K is $E_{mp} = 205$ cm^{-1}, and the full width at half-maximum of the distribution is $\Delta E_{fwhm} \cong 500$ cm^{-1}.

In addition to the experimentally determined total removal rate constants, Table 1 presents the computed total removal rate constants. Three calculations are presented: The first are full calculations, with inclusion of the isolated-molecule non-Born−Oppenheimer mixing and the V_1 coupling PES. The non-Born−Oppenheimer mixing includes the spin−orbit, orbit−rotation, and spin−rotation coupling (see p 124 of ref 5) with magnitudes appropriate to the isolated CN molecule.[9] To investigate the relative effect of the coupling PES vs the gateway effect in inducing collision-induced electronic transitions, we determined a second set of total removal rates constants from calculations in which V_1 was set to zero but in which the non-Born−Oppenheimer mixing in the isolated molecule was retained. Finally, we tabulate the total removal rates are from our previously reported[33] calculations for $N = 60$ initial levels, which considered only collision-induced rotational transitions within the A state (V_Π and V_2 PESs only).

As noted previously,[33] the rate constants for the sum of all rotationally inelastic transitions out of $N = 60$ initial levels are slightly larger for A″ than for A′ Λ-doublets. The total removal rate constants obtained from full calculations for the F_1e (A′) and F_1f (A″) initial levels are slightly larger than those for where only rotational energy transfer within the A state was considered and show an enhancement in the rate constant for the A″ initial Λ-doublet level.

TABLE 3: Computed Relative State-to-State Rate Constants[a] for A → X Electronic Transitions from CN($A^2\Pi$,v=3,N) Fine-Structure/Λ-Doublet Levels Induced by Collisions with Ar

	initial fine-structure/Λ-doublet level			
	F_1e		F_1f	
final level	full calc	$V_1 = 0$	full calc	$V_1 = 0$
	$N = 60$ Initial Levels			
$N' = 59$				
F_1	*b*	*b*	*b*	*b*
F_2	0.004	*b*	0.007	*b*
$N' = 60$				
F_1	*b*	*b*	0.004	*b*
F_2	0.012	*b*	0.152	*b*
$N' = 61$				
F_1	0.012	*b*	0.003	*b*
F_2	0.714	*b*	0.102	0.036
$N' = 62$				
F_1	0.003	*b*	*b*	*b*
F_2	0.047	0.006	0.199	0.002
	$N = 62$ Initial Levels			
$N' = 61$				
F_1	*b*	*b*	*b*	*b*
F_2	0.006	*b*	0.015	0.005
$N' = 62$				
F_1	*b*	*b*	0.002	*b*
F_2	0.020	*b*	0.349	0.016
$N' = 63$				
F_1	0.017	0.003	0.006	0.002
F_2	2.540	0.007	3.136	3.750
$N' = 64$				
F_1	0.002	*b*	*b*	*b*
F_2	0.077	0.010	0.082	0.019

[a] Normalized to the $\Delta N = -1$ fine-structure and Λ-doublet symmetry conserving collision-induced pure rotational transition within the $v_A = 3$ manifold. [b] Relative rate constant <0.001.

The total removal rate constants obtained from full calculations for the $N = 62$ F_1e and F_1f initial levels are significantly larger than the values for the corresponding $N = 60$ levels. We note that the perturbed $N = 62$ F_1f initial level has the largest computed total removal rate constant of the levels investigated. The total removal rate constants computed with V_1 set to zero show an even larger enhancement for the perturbed $N = 62$ F_1f level. Surprisingly, the total removal rate constants computed with V_1 set to zero for the $N = 60$ F_1e and F_1f initial levels are slightly smaller than those computed with consideration of only collision-induced rotational transitions within the A state. This indicates that the electronic and rotational inelasticities interfere, to some extent, and are not simply additive.

It is also of interest to examine computed state-to-state A → X rate constants. Table 3 presents relative rate constants from the $N = 60$ and 62 F_1e and F_1f initial levels, obtained from calculations with the full set of PESs and from those in which the V_1 coupling PES was set to zero. The rate constants are nonnegligible for only a small range of final rotational levels N'. Consequently, only these transitions are listed in Table 3. Also computed but not presented in Table 3 were state-to-state rate constants for collision-induced rotational transitions within the A state. As noted earlier, these had previously[33] been computed for $N = 60$ initial levels by consideration of the interaction of the A state with the atomic collision partner (V_Π and V_2 PESs only). We find only slight differences in the state-

to-state rate constants for collision-induced rotational transitions resulting from the two sets of calculations.

In the calculations of the state-to-state A → X rate constants computed with the V_1 PES, there is a strong propensity for all initial levels toward population of the F_2 fine-structure level for a given rotational level N' in the $v_X = 7$ vibronic manifold. This contrasts with our experimental observation for $N = 60$ initial levels (see Table 2) of conservation of the fine-structure label in collisional A → X transitions whose state-to-state rate constants are large enough that the final level could be detected. It should be noted that the most strongly perturbed $v_X = 7$ level is an F_2 level, and perhaps this preference for formation of F_2 final levels is a manifestation of the "gateway" effect in the calculations. We also do not find in the calculations with the V_1 PES the Λ-doublet propensities seen in the experimentally determined A → X rate constants out of the relatively unperturbed $N = 60$ initial levels, wherein the final rotational levels populated resulted from changes $\Delta N = +1$ and 0 for initial Λ-doublet levels of A′ and A″ symmetry, respectively; this propensity is observed for the F_1e initial level, but not F_1f.

The calculations with the V_1 PES for $N = 62$ initial levels do show prominently the effect of the gateway. The calculated rate constants are very large for formation of the $N = 63$ F_2 final level, i.e., the most $v_X = 7$ perturbed level. The computed relative rate constants are actually significantly larger than the corresponding experimental rate constants. The state-to-state rate constants computed with the V_1 coupling PES set to zero provide an opportunity to separate the effect of the V_1 coupling PES and the spectroscopic "gateway". We see from Table 3 that the state-to-state computed rate constants for the relatively unperturbed $N = 60$ F_1e and F_1f and $N = 62$ F_1e initial levels are negligible when V_1 is set to zero. Also, the state-to-state A → X rate constant for the perturbed $N = 62$ F_1f initial level is large only for the transition to the perturbed $N = 63$ F_2 final level (the "gateway" to "gateway" transition).

The striking differences in the rate constants obtained from the two sets of calculations indicate that the spectroscopic "gateway" is very important in enabling collision-induced electronic transitions. In addition, the electrostatic coupling between the $A^2\Pi$ and $X^2\Sigma^+$ states, represented by the V_1 coupling PES, also contributes significantly by allowing transitions to and from levels that are not strongly affected by the spectroscopic perturbation.

4. Discussion

We have presented a collaborative experimental and theoretical study of A → X electronic transitions from CN($A^2\Pi$,v=3,N=60−63) fine-structure/Λ-doublet levels induced by collisions with argon and helium. For this high level of rotational excitation, the CN(A) electronic state approaches the Hund's case (b) limit, in which the electron spin is weakly coupled to the diatomic internuclear axis.[39] Moreover, the spacings between successive rotational levels N are comparable to kT, unlike the situation for the low CN rotational levels. As a result, the state-to-state rate constants show a qualitatively different dependence upon the quantum numbers of the final levels than seen in our previous investigation[26] of collision-induced electronic transitions from low rotational levels of the $v_A = 3$ manifold.

For low-J initial levels, the final rotational level distribution in the $v_X = 7$ manifold displayed an even−odd alternation as a function of the final rotational angular momentum N'. This oscillation could be attributed to the near homonuclear character of the CN($X^2\Sigma^+$,$A^2\Pi$)Ar PESs,[32] in particular the V_1 coupling PES. Such an oscillation in the final state populations is not observed here for high initial rotational levels, presumably because of the large rotational spacings and the consequent rapid decrease in the rate constants with increasing change in the rotational angular momentum. A similar loss of alternation was observed in rotationally inelastic collisions within high-J levels of the A state.[33]

Our particular focus in this study has been the investigation of the relative importance for high rotational levels of CN($A^2\Pi$) of the two mechanisms invoked to describe collision-induced electronic transitions,[3] namely "gateways" caused by perturbational mixing in the isolated diatomic molecule[4] and electrostatic mixing of the diatom electronic states induced by the approach of the collision partner.[8] To this end, we have determined total removal and state-to-state A → X rate constants for $v_A = 3$ initial levels near the spectroscopic perturbation with the $v_X = 7$ manifold at $J = 62.5$ in collisions with Ar and He. The enhanced efficiency of electronic energy transfer for a spectroscopically perturbed "gateway" level was seen in the significantly larger total removal rate constant for the $N = 62$ F_1f level ($J = 62.5$) for CN(A)−Ar collisions as compared to the total removal rate constants for other initial levels with similar total internal energy. The role of the gateway was also in evidence in the state-to-state A → X rate constants, as the rate constant from this initial level to the corresponding perturbed level in the $v_X = 7$ manifold ($N = 63$ F_2) was found to be large.

The experimentally determined CN−Ar rate constants were compared with theoretical rate constants computed on the basis of ab initio CN($X^2\Sigma^+$,$A^2\Pi$)Ar PESs.[32] The computed total removal rate constants do display an enhanced value for the perturbed $N = 62$ F_1f initial level, in agreement with experiment. However, the agreement of the computed state-to-state rate constants for the $N = 60$ and 62 F_1e and F_1f initial levels with the experimental values is disappointing. In particular, the experimentally observed conservation of the fine-structure label, i.e., the coupling of **N** and **S** to form the total angular momentum **J**, was not reproduced in the computed state-to-state rate constants. In contrast, we found excellent agreement between theory and experiment for state-to-state rate constants for collision-induced rotational transitions involving collisions of CN($A^2\Pi$) with both Ar and He.[33,34]

The true V_1 coupling potential depends not only on the orientation of the CN molecule relative to the atomic partner but also on the CN bond distance r. In the earlier investigation of the CNHe PESs,[30] the V_1 PES was determined at several values of r and then averaged over the product of the vibrational wave functions of the $v_A = 3$ and $v_X = 7$ vibronic levels. In contrast, the more recent calculations of the CNAr PESs by Berning and Werner[32,49] were limited to a single value of r. The averaging over the products of the vibrational wave functions in the two electronic states was done by multiplying the calculated value of V_1 (at this single value of r) by the $v_A = 3/v_X = 7$ Franck−Condon factor. A more complete MRCI calculation of the PESs, followed by a correct averaging over r, could well resolve the discrepancy with experiment seen here.

To unravel the relative importance of the two mechanisms for electronic energy transfer in the computed rate constants, values obtained in the full calculations have been compared with those computed with the V_1 coupling PES set to zero. In the latter set of calculations, the only A → X state-to-state rate constant of significant magnitude was for the transition from the perturbed level in the A state ($N = 62$ F_1f) to the perturbed level in the X state ($N = 63$ F_2), i.e., a transition between the two "gateway" levels. This clearly differs from the qualitative

appearance of the experimentally determined state-to-state rate constants, for which significant values are observed for transitions between unperturbed levels. We thus conclude that both mechanisms are operating in electronic transitions involving high rotational levels of CN($A^2\Pi$) induced by collisions with Ar.

Our calculations, which were based on realistic PESs and an excellent treatment of the collision dynamics, predict that the gateway contribution to electronic energy transfer in CN, although large, does not completely dominate the contribution due to direct collisional coupling of the levels in question. This stands in contrast to other, earlier predictions, based on more approximate treatments of the interaction potentials and the collision dynamics, which predict that gateway transfer will be 1−2 orders of magnitude more efficient.[50,51]

From the examination of the disagreement of the experimental and computed CN(A)−Ar state-to-state rate constants, it appears that the role of the gateways has been overemphasized in the calculations. This could be due to inaccuracies in the V_1 coupling PES, which were discussed earlier in this section. Another possible source of error is our treatment of the electronic state mixing (the non Born−Oppenheimer couplings) in the isolated CN radical. We have assumed that this mixing is independent of the approach of the collision partner. This is likely an excellent approximation, since thermal energy collisions will sample only the relatively long-range part of the CN−Ar interaction. At these distances the perturbation of the electron clouds is small, so that the expectation of the electronic orbital angular momentum and its projections (which enter into the magnitude of the non-Born−Oppenheimer couplings) will be little affected. Although the variation of these couplings with the CN−Ar distance was not explored by Berning,[49] similar studies of the H−Cl, F−H_2, and Cl−H_2 systems[52−54] suggest strongly that the variation with distance of these constants will be small, over the range of distances sampled in the collision.

Collision-induced A → X electronic transitions with helium as the collision partner have been found to be significantly less facile than for collisions with Ar. This difference also points to the role of the V_1 coupling PES, rather than the spectroscopic "gateways", in enabling the collision-induced electronic transitions, since the magnitude of the isolated-molecule non-Born−Oppenheimer mixing is independent of the identity of the collision partner. In ab initio calculations of the interaction potentials, the V_1 coupling PES was found to be considerably smaller for the CN($X^2\Sigma^+$,$A^2\Pi$)He than CN($X^2\Sigma^+$,$A^2\Pi$)Ar system.[30,32] This difference in the coupling strength can explain the altered magnitude of the CN A → X rate constants involving collisions of Ar and He.

In this state-to-state study of collision-induced electronic transitions involving high rotational levels of the CN radical, we thus find that both mechanisms play a role in inducing transitions from the $A^2\Pi$ to $X^2\Sigma^+$ electronic state. The relative importance of the "gateway" and collision-induced electrostatic mixing mechanisms depends on the degree of mixed electronic state character of the rotational levels involved.

Acknowledgment. This research has been supported by the National Science Foundation under Grant No. CHE-9971810.

Appendix: CN B−A and B−X Line Strength Factors

The determination of the ratios of rate constants for collision-induced A → X electronic transitions and collision-induced rotational transitions within the A state depend on accurate measurement of populations of rotational levels within the A and X electronic states. We provide a brief discussion of the intensity factors used to convert B−A and B−X laser-induced fluorescence signals to populations in the A and X states, respectively. On the basis of multireference configuration interaction calculations of the CN electronic states, Knowles et al.[36] have provided tables of radiative transition probabilities for B−A and B−X bands. These calculations provide CN($A^2\Pi$ and $B^2\Sigma^+$,v) radiative lifetimes that are in good agreement with experiment.

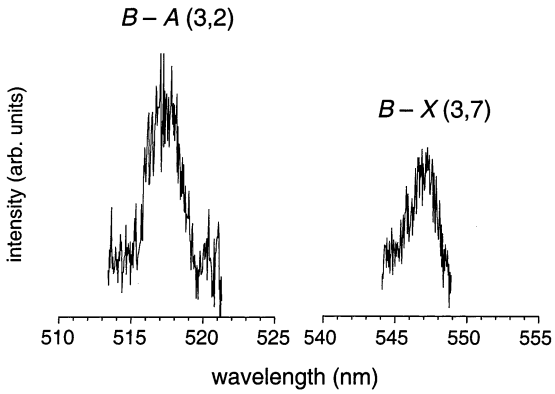

Figure 7. Fluorescence spectrum in the B → A (3,2) and B → X (3,7) bands upon probe laser excitation in the B−A (3,3) $P_2(6)$ line after pump laser excitation in the A−X (3,0) R_2 band head in the presence of 900 mTorr He. The photolysis−pump and pump−probe delays were 100 μs and 30 ns, respectively.

Because of the large angular momenta of the rotational levels studied here and the expected effect of the centrifugal potential on vibrational overlap integrals, we have recalculated the band strengths using the ab initio transition moment functions[36] and RKR potential energy curves,[11] with inclusion of the centrifugal potential. We find that the ratio of the electric dipole transition matrix elements, $m(v_B=3,v_X=7)/m(v_B=3,v_A=3)$, equals +0.43 for rotational angular momentum $N = 62$. This value is 15% larger than for $N = 0$. The transition moments are defined following the recommendations of Whiting et al.[55] The phase of the ratio of transition moments for the CN B−A and B−X bands has been determined previously.[41] The B−A and B−X fluorescence excitation intensity factors for individual rotational lines were computed using the rotational line strength factor defined in eq 7 of ref 41.

Comparison of lifetimes does not provide a sensitive check on the computed[36] B → A transition rates, and hence the B−A transition moment, since the $B^2\Sigma^+$ state decays primarily through B → X fluorescence. We have recorded fluorescence emission spectra to check that the calculated B−A band strengths are accurate. The probe laser wavenumber was set to that of the B−A (3,3) $P_2(6)$ line, with a long photolysis−pump delay so that the rotational state distribution was thermalized.[56] Population within the A state was prepared by pump laser excitation of the A−X (3,0) R_2 band head. Excitation of low rotational levels, rather than high-N levels, is advantageous because of the significantly larger fluorescence signals for the former, with a thermalized sample.

We desire to measure the ratio of the B → A (3,3) and B → X (3,7) band intensities. However, it was not possible to observe emission in the B−A (3,3) band because of scattered laser light. Instead, we chose to compare the intensities of the B → A (3,2) and B → X (3,7) bands, which occur at 516 and 546 nm, respectively. The response of the fluorescence detection system in this small wavelength range is constant. A color filter was used to block the very strong emission in the B → X (3,3) band. A fluorescence emission spectrum is displayed in Figure 7. The computed[36] Einstein spontaneous emission probabilities are 2.81

$\times 10^3$ and 1.51×10^3 s^{-1} for the B → A (3,2) and B → X (3,7) bands, respectively, yielding a calculated band intensity ratio of 1.87. From spectra such as that shown in Figure 7, the experimentally measured ratio is 1.45. The difference in the computed and measured intensity ratio is less than 30%, which is close to our estimated experimental uncertainty in the measurement of OODR line intensities.

References and Notes

(1) Kohse-Höinghaus, K. *Prog. Energy Combust. Sci.* **1994**, *20*, 203.
(2) Crosley, D. R. In *Current Problems and Progress in Atmospheric Chemistry*; Barker, J. R., Ed.; World Scientific: Singapore, 1996; p 256.
(3) Dagdigian, P. J. *Annu. Rev. Phys. Chem.* **1997**, *48*, 95.
(4) Gelbart, W. M.; Freed, K. F. *Chem. Phys. Lett.* **1973**, *18*, 470.
(5) Lefebvre-Brion, H.; Field, R. W. *Perturbations in the Spectra of Diatomic Molecules*; Academic: Orlando, FL, 1986.
(6) Dagdigian, P. J. In *The Chemical Dynamics and Kinetics of Small Radicals, Part I*; Liu, K., Wagner, A. F., Eds.; World Scientific: Singapore, 1995; p 315.
(7) Schiffman, A.; Chandler, D. W. *Int. Rev. Phys. Chem.* **1995**, *14*, 371.
(8) Alexander, M. H.; Corey, G. C. *J. Chem. Phys.* **1986**, *84*, 100.
(9) Kotlar, A. J.; Field, R. W.; Steinfeld, J. I.; Coxon, J. A. *J. Mol. Spectrosc.* **1980**, *80*, 86.
(10) Prasad, C. V. V.; Bernath, P. F.; Frum, C.; Engelman Jr., R. *J. Mol. Spectrosc.* **1992**, *151*, 459.
(11) Prasad, C. V. V.; Bernath, P. F. *J. Mol. Spectrosc.* **1992**, *156*, 327.
(12) Rehfuss, B. D.; Suh, M. H.; Miller, T. A.; Bondybey, V. E. *J. Mol. Spectrosc.* **1992**, *151*, 437.
(13) Katayama, D. H.; Dentamaro, A. V. *J. Chem. Phys.* **1989**, *91*, 4571.
(14) Katayama, D. H.; Dentamaro, A. V. *J. Chem. Phys.* **1986**, *85*, 2595.
(15) Katayama, D. H. *J. Chem. Phys.* **1984**, *81*, 3495.
(16) Berning, A.; Werner, H.-J. *J. Chem. Phys.* **1994**, *100*, 1953.
(17) Pratt, D. W.; Broida, H. P. *J. Chem. Phys.* **1969**, *50*, 2181.
(18) Bondybey, V. E. *J. Chem. Phys.* **1977**, *66*, 995.
(19) Lawrence, W. G.; Chen, Y.; Heaven, M. C. *J. Chem. Phys.* **1997**, *107*, 7163.
(20) Yang, M.; Alexander, M. H. *J. Chem. Phys.* **1997**, *107*, 7148.
(21) Lin, H.-S.; Erickson, M. G.; Lin, Y.; Basinger, W. H.; Lawrence, W. G.; Heaven, M. C. *Chem. Phys.* **1994**, *189*, 235.
(22) Katayama, D. H.; Miller, T. A.; Bondybey, V. E. *J. Chem. Phys.* **1979**, *71*, 1662.
(23) Halpern, J. B.; Wang, Y. In *Research in Chemical Kinetics*; Compton, R. G., Hancock, G., Eds.; Elsevier: Amsterdam, 1993; Vol. 1, p 347.
(24) Furio, N.; Ali, A.; Dagdigian, P. J. *Chem. Phys. Lett.* **1986**, *125*, 561.
(25) Furio, N.; Ali, A.; Dagdigian, P. J. *J. Chem. Phys.* **1986**, *85*, 3860.
(26) Jihua, G.; Ali, A.; Dagdigian, P. J. *J. Chem. Phys.* **1986**, *85*, 7098.
(27) Ali, A.; Jihua, G.; Dagdigian, P. J. *J. Chem. Phys.* **1987**, *87*, 2045.
(28) Dagdigian, P. J.; Patel-Misra, D.; Berning, A.; Werner, H.-J.; Alexander, M. H. *J. Chem. Phys.* **1993**, *98*, 8580.
(29) Davis, S. P.; Phillips, J. G. *The Red System ($A^2\Pi - X^2\Sigma$) of the CN Molecule*; University of California Press: Berkeley, CA, 1963.
(30) Werner, H.-J.; Follmeg, B.; Alexander, M. H. *J. Chem. Phys.* **1988**, *89*, 3139.
(31) Werner, H.-J.; Follmeg, B.; Alexander, M. H.; Lemoine, D. *J. Chem. Phys.* **1989**, *91*, 5425.
(32) Alexander, M. H.; Yang, X.; Dagdigian, P. J.; Berning, A.; Werner, H.-J. *J. Chem. Phys.* **2000**, *112*, 781.
(33) Yang, X.; Dagdigian, P. J.; Alexander, M. H. *J. Chem. Phys.* **2000**, *112*, 4474.
(34) Nizamov, B.; Dagdigian, P. J.; Alexander, M. H. *J. Chem. Phys.* **2001**, *115*, 8393.
(35) Wright, S. A.; Dagdigian, P. J. *J. Chem. Phys.* **1995**, *103*, 6479.
(36) Knowles, P. J.; Werner, H.-J.; Hay, P. J.; Cartwright, D. C. *J. Chem. Phys.* **1988**, *89*, 7334.
(37) Alexander, M. H.; Andresen, P.; Bacis, R.; Bersohn, R.; Comes, F. J.; Dagdigian, P. J.; Dixon, R. N.; Field, R. W.; Flynn, G. W.; Gericke, K.-H.; Grant, E. R.; Howard, B. J.; Huber, J. R.; King, D. S.; Kinsey, J. L.; Kleinermanns, K.; Kuchitsu, K.; Luntz, A. C.; MacCaffery, A. J.; Pouilly, B.; Reisler, H.; Rosenwaks, S.; Rothe, E.; Shapiro, M.; Simons, J. P.; Vasudev, R.; Wiesenfeld, J. R.; Wittig, C.; Zare, R. N. *J. Chem. Phys.* **1988**, *89*, 1749.
(38) Yang, X.; Dagdigian, P. J. *J. Mol. Spectrosc.* **1999**, *198*, 189.
(39) Herzberg, G. *Molecular Spectra and Molecular Structure I. Spectra of Diatomic Molecules*, 2nd ed.; D. Van Nostrand: Princeton, NJ, 1950.
(40) Hay, S.; Shokoohi, F.; Callister, S.; Wittig, C. *Chem. Phys. Lett.* **1985**, *118*, 6.
(41) Furio, N.; Ali, A.; Dagdigian, P. J.; Werner, H.-J. *J. Mol. Spectrosc.* **1989**, *134*, 199.
(42) Corey, G. C.; Alexander, M. H. *J. Chem. Phys.* **1986**, *85*, 5652.
(43) Kouri, D. J. In *Atom-Molecule Collision Theory: A Guide for the Experimentalist*; Bernstein, R. B., Ed.; Plenum: New York, 1979; p 301.
(44) McGuire, P.; Kouri, D. J. *J. Chem. Phys.* **1974**, *60*, 2488.
(45) Pack, R. T *J. Chem. Phys.* **1974**, *60*, 633.
(46) Alexander, M. H.; Gregurick, S.; Dagdigian, P. J. *J. Chem. Phys.* **1994**, *101*, 2887.
(47) Smith, I. W. M. *Kinetics and Dynamics of Elementary Gas Reactions*; Butterworth: London, 1980.
(48) HIBRIDON is a package of programs for the time-independent quantum treatment of inelastic collisions and photodissociation written by M. H. Alexander, D. E. Manolopoulos, H.-J. Werner, and B. Follmeg, with contributions by P. F. Vohralik, D. Lemoine, G. Corey, B. Johnson, T. Orlikowski, W. Kearney, A. Berning, A. Degli-Esposti, C. Rist, and P. J. Dagdigian. More information and/or a copy of the code can be obtained from the website http://www-mha.umd.edu/~mha/hibridon.
(49) Berning, A. Energieübertragungsprozesse in Atom-Molekül Stössen. Ph.D., Universität Stuttgart, 1995.
(50) Alexander, M. H.; Osmolovsky, M. G. *J. Chem. Phys.* **1982**, *77*, 839.
(51) Pouilly, B.; Robbe, J.-M.; Alexander, M. H. *J. Phys. Chem.* **1984**, *88*, 140.
(52) Alexander, M. H.; Pouilly, B.; Duhoo, T. *J. Chem. Phys.* **1993**, *99*, 1752.
(53) Stark, K.; Werner, H.-J. *J. Chem. Phys.* **1996**, *104*, 6515.
(54) Capecchi, G.; Werner, H.-J.. To be published.
(55) Whiting, E. E.; Schadee, A.; Tatum, J. B.; Hougen, J. T.; Nicholls, R. W. *J. Mol. Spectrosc.* **1980**, *80*, 249.
(56) Nizamov, B.; Dagdigian, P. J.; Tzeng, Y.-R.; Alexander, M. H. *J. Chem. Phys.* **2001**, *115*, 800.